STEAM TURBINE MATERIALS AND CORROSION

Gordon R. Holcomb
National Energy Technology Laboratory, 1450 Queen Ave SW, Albany, OR 97321
Email: Gordon.Holcomb@netl.doe.gov; Voice: (541) 967-5874; Fax: (541)-967-5914

Derek Hsu
National Energy Technology Laboratory, 1450 Queen Ave SW, Albany, OR 97321
Email: Derek.Hsu@or.netl.doe.gov; Voice: (541) 967-5893; Fax: 541-967-5991

ABSTRACT

Ultra-supercritical (USC) power plants offer the promise of higher efficiencies and lower emissions. Current goals of the U.S. Department of Energy's Advanced Power Systems Initiatives include coal generation at 60% efficiency, which would require steam temperatures of up to 760 °C. In prior years this project examined the steamside oxidation of alloys for use in high- and intermediate-pressure USC turbines. This steamside oxidation research is continuing and progress is presented, with emphasis on chromia evaporation.

INTRODUCTION

Goals of the U.S. Department of Energy's Advanced Power Systems Initiatives include power generation from coal at 60% efficiency, which requires steam conditions of up to 760 °C and 340 atm, so called ultra-supercritical (USC) steam conditions. A limitation to achieving the goal is a lack of cost-effective metallic materials that can perform at these temperatures and pressures. Some of the more important performance limitations are high-temperature creep strength, fire-side corrosion resistance, and steam-side oxidation resistance. Nickel-base superalloys are expected to be the materials best suited for steam boiler and turbine applications above about 675 °C].[1] Specific alloys of interest include Haynes 230 and 282, Inconel 617, 625, 718, and 740, Nimonic 105, and Udimet 720Li. Alloy compositions are given in Table 1.

Steam-side oxidation can result in several adverse conditions: general section loss from material thinning, deep localized section loss from internal oxidation (that may also provide crack initiation sites), dimensional changes that are critical in airfoils, and downstream erosion from oxide spallation. Evaporation of protective chromia scales may also be an issue at the higher temperatures and pressures of USC steam turbines. The evaporation of chromia scales in steam is the focus of the research presented here.

In prior work, a methodology to calculate the expected chromia evaporation rate as a function of temperature, pressure, gas velocity, and steam chemistry was developed[2] for chromia-forming alloys used as steam turbine blades. The methodology was experimentally validated at low pressures and gas velocities by how well its kinetics predictions matched atmospheric pressure oxidation experiments in air plus water vapor environments. At 760 °C and 340 atm, evaporation rates as high as 5.18×10^{-8} kg/m^2/s of $CrO_2(OH)_2(g)$ were predicted for rotating high pressure (HP) turbine blade components.[2] It was speculated that chromia evaporation upstream of the HP turbine, such as in the superheater, could partially saturate the steam with $CrO_2(OH)_2(g)$ and reduce the chromia evaporation rate.

The research presented here expands upon the prior work by 1) expanding the methodology from flat plate components to cylindrical geometries (such as found within superheaters and steam pipes), 2) linking the chromia evaporation in steam to Cr diffusion within the alloy to predict alloy Cr concentration profiles and breakaway oxidation times, 3) comparing these predictions to Cr concentration profiles found in laboratory experiments, and 4) applying the breakaway oxidation predictions to a hypothetical superheater-steam pipe-HP turbine steam path, where the effects of $CrO_2(OH)_2(g)$ saturation along the steam path are applied.

Table 1. Alloy Composition*, Density, and Bulk Alloy Cr Concentration (C_{Cr}°) for alloys of interest.[3-10]

Alloy	Fe	Cr	Ni	Co	Mo	C	Si	Ti	Al	B ppm	Mn	Other	Density g/cm^3	C_{Cr}° mol/m^3
Haynes 230	1.5	22	Bal	2.5	2	0.1	0.4		0.3	75	0.5	0.02 La 14 W	8.97	0.0380
Haynes 282	0.75	19.5	Bal	10	8.5	0.06	0.075	2.1	1.5	50		0.15 Cu	8.27	0.0310
Inconel 617	1.5	22	Bal	12.5	9	0.1	0.5	0.3	1.15	30	0.5	0.25 Cu	8.36	0.0354
Inconel 625	2.5	21.5	Bal	0.5	9	0.05	0.25	0.2	0.2		0.25	3.65 Nb	8.44	0.0349
Inconel 718	Bal	19	52	0.5	3.05	0.04	0.175	0.9	0.5	30	0.175	5.125 Nb 0.15 Cu	8.19	0.0299
Inconel 740	0.7	25	Bal	20	0.5	0.03	0.5	1.8	0.9		0.3	2 Nb	8.05	0.0387
Nimonic 105	0.5	14.85	Bal	20	5	0.085	0.5	1.2	4.7	65	0.5	0.075 Zr 0.1 Cu	8.01	0.0229
Udimet 720Li		16	Bal	14.75	3	0.015		5	2.5	150		1.25 W 0.0375 Zr	8.08	0.0249

*Source values that were ranges are listed as the midpoint of the range. Source values that were maximums are listed as half the maximum. Only Nb is listed for sources that gave a value or range for Nb+Ta. Source values for Pb, P, and S are omitted.

CHROMIA EVAPORATION

The oxidation of alloys protected by the formation of Cr_2O_3 (chromia formers) can undergo scale loss due to reactive evaporation of chromium-containing gas species. Water vapor increases the evaporation loss by allowing the formation of $CrO_2(OH)_2$(g), which for these conditions has a higher vapor pressure than CrO_3(g). CrO_3(g) is the predominate Cr gas specie in dry air or oxygen. The formation of $CrO_2(OH)_2$(g) can be written as:

$$\tfrac{1}{2}Cr_2O_3(s) + H_2O(g) + \tfrac{3}{4}O_2(g) = CrO_2(OH)_2(g) \qquad (1)$$

Evaporation can change the overall oxidation kinetics from parabolic behavior to linear kinetics or even to breakaway oxidation. Linear kinetics can arise after scale growth from oxidation, which decreases with increasing scale thickness, matches the scale loss from reactive evaporation. The change in scale thickness, x, with time, t, can then be described in terms of the parabolic rate constant, k_p, and the linear reactive evaporation rate, k_e, as:

$$\frac{dx}{dt} = \frac{k_p}{x} - k_e \qquad (2)$$

At long times or high reactive evaporation rates, a limiting scale thickness, x_L, arises that is given by:

$$x_L = \frac{k_p}{k_e} \qquad (3)$$

In this case metal loss rates are linear, but still involve diffusion through a protective scale. Rapid metal loss can occur when reactive evaporation of Cr depletes the scale (and sometimes the substrate metal) of Cr.[11-12] Decreased Cr in the scale or metal can lead to the formation of less protective oxides, such as Fe-Cr oxides in Fe-Cr base alloys. Unprotective scales can lead to rapid metal loss, or "break-away" oxidation.

A detailed methodology for calculating evaporation rates in a variety of environments was presented in earlier work[2] for gas flow over a flat plate. Two basic equations were developed: Eq. 4 for laminar flow and Eq. 5 for turbulent flow:

$$k_e\left(\tfrac{kg}{m^2 s}\right) = 0.664\, Re_L^{0.5} Sc^{0.343} \frac{D_{AB} M_{CrO_2(OH)_2}}{LRT} P_{CrO_2(OH)_2} \tag{4}$$

$$k_e\left(\tfrac{kg}{m^2 s}\right) = 0.0592\, Re_L^{0.8} Sc^{0.333} \frac{D_{AB} M_{CrO_2(OH)_2}}{LRT} P_{CrO_2(OH)_2} \tag{5}$$

where Re_L and Sc are the dimensionless Reynolds and Schmidt numbers, D_{AB} is the gaseous diffusion coefficient between $CrO_2(OH)_2$ and the solvent gas (m^2/s), $M_{CrO2(OH)2}$ is the molecular mass of $CrO_2(OH)_2$ (kg/g-mol), L is the length (m) in the flow direction of the flat plate, $P_{CrO2(OH)2}$ is the partial pressure of $CrO_2(OH)_2$ (atm), R is the gas constant (8.20594×10^{-5} m^3atm/K g-mol), and T is the absolute temperature (K). The dimensionless Reynolds and Schmidt numbers are defined as:

$$Re_L = \frac{\rho_s u L}{\eta} \tag{6}$$

$$Sc = \frac{\eta}{\rho_s D_{AB}} \tag{7}$$

where ρ_s is the density of the solvent gas (kg/m^3), η is the absolute viscosity (kg/m/s), and u is the gas velocity (m/s). The Gibbs energy for reaction 1 was used to determine $P_{CrO2(OH)2,}$ and the Gindorf *et al.* data[13] for the formation of $CrO_2(OH)_2$(g) was found to best agree with experimental oxidation kinetics.[2]

In order to later expand the above methodology for use in pipes and to include possible saturation effects, it is useful to rewrite Eqs. 4-5 in more general terms that include the average Sherwood number (Sh_{Ave}) and to allow for the value of the partial pressure of $CrO_2(OH)_2$(g) well away from the metal surface, $P_{CrO2(OH)2}^{\circ}$, to slow down the evaporation (Eqs. 4-5 assumed $P_{CrO2(OH)2}^{\circ}$ was zero):

$$k_e\left(\tfrac{kg}{m^2 s}\right) = Sh_{Ave} \frac{D_{AB} M_{CrO_2(OH)_2}}{LRT} \left(P_{CrO_2(OH)_2} - P^{\circ}_{CrO_2(OH)_2}\right) \tag{8}$$

where Sh_{Ave} is equal to $0.664Re_L^{0.5}Sc^{0.343}$ for laminar flow over flat plates and to $0.0592Re_L^{0.8}Sc^{0.333}$ for turbulent flow over flat plates.

For flow within circular tubes, Eq. 8 is used but with different expressions for Sh_{Ave}. For the analysis that follows, the Dittus-Boelter equation[14-15] was used for Sh_{Ave} for turbulent conditions:

$$Sh_{Ave} = 0.023 Re_d^{0.8} Sc^{0.4} \tag{9}$$

where Re_d is the same as Re_L but with the diameter, d, instead of the plate length, L, in Eq. 6. For rough pipes the use of an expression for Sh_{Ave} that incorporates a friction factor, such as that of Petukov[15-16] can be used.

CHROMIUM DIFFUSION

After evaporation causes the overall oxidation kinetics to become linear and to have a steady state scale thickness (Eq. 3), the flux of Cr away from the scale via evaporation must equal the flux of Cr to the scale via Cr diffusion within the alloy. If there is insufficient arrival of Cr to the surface, then the chromia scale will not be maintained and breakaway oxidation would be expected to eventually occur.

To model Cr diffusion within the alloy with a constant flux of Cr leaving the surface, the transient heat transfer model of Incropera and DeWitt[15] within a semi-infinite solid and with a constant surface heat flux was used. The underlying mathematics between heat and mass transfer are the same, and so this model could be used with appropriate mass transfer parameters. The overall equation for the concentration of Cr as a function of x (depth from the surface into the alloy, m) and t (time, s), $C_{Cr}(x,t)$ is:

$$C_{Cr}(x,t) = C^{\circ}_{Cr} - \frac{2k_e}{M_{CrO_2(OH)_2}}\sqrt{\frac{t}{\pi D_{Cr}}}\exp\left(-\frac{x^2}{4D_{Cr}t}\right) + \frac{k_e x}{M_{CrO_2(OH)_2}D_{Cr}}\operatorname{erfc}\left(\frac{x}{2\sqrt{D_{Cr}t}}\right) \qquad (10)$$

where C_{Cr}° is the bulk alloy Cr concentration (mol/m^3), D_{Cr} is the diffusion coefficient of Cr (m^2/s), and erfc is the complementary error function. For the concentration of Cr at the surface as a function of time, Eq. 10 simplifies to:

$$C_{Cr}(0,t) = C^{\circ}_{Cr} - \frac{2k_e}{M_{CrO_2(OH)_2}}\sqrt{\frac{t}{\pi D_{Cr}}} \qquad (11)$$

And the surface concentration is equal to zero at time t^*:

$$t^* = \frac{\pi D_{Cr}}{4}\left(\frac{M_{CrO_2(OH)_2}C^{\circ}_{Cr}}{k_e}\right)^2 \qquad (12)$$

Breakaway oxidation would be expected to occur prior to t^*, such as when the surface concentration becomes less than some critical value. There is no universally accepted critical surface concentration, but it cannot be less than zero. So t^* is used as a proxy for the time until breakaway oxidation will occur.

At the temperatures in a steam turbine, the diffusion coefficient, D_{Cr}, is an effective diffusion coefficient and is a combination of lattice, D_{Cr}^{L}, and grain boundary, D_{Cr}^{gb}, diffusion. The relationship used[17] is based on cubic grains of size λ (m) and with grain boundary width δ (m):

$$D_{Cr} \cong D^{L}_{Cr} + \frac{2\delta}{\lambda}D^{gb}_{Cr} \qquad (13)$$

The lattice diffusion coefficients were determined using Dictra diffusion simulation software[18] with the Ni-DATA[19] and MOB2 (ref 20) databases. Figure 1 shows lattice diffusion coefficients of Cr in the face-centered cubic (FCC) phase for alloys of interest as a function of Cr content at 760 °C. The right-most-point for each alloy is at the alloy Cr content. The lower Cr content values represent the alloy where it is locally depleted in Cr near the surface. Figure 1 shows that for many of the alloys, an assumption of a constant value for the diffusion coefficient is a good one.

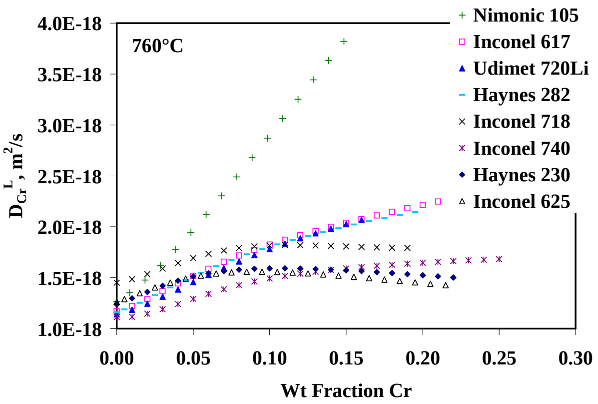

Figure 1. Lattice diffusion coefficients at 760 °C for Cr in the FCC phase of nickel base superalloys determined using Dictra diffusion simulation software[18] with the Ni-DATA[19] and MOB2 (ref 20) databases.

The use of the FCC phase as the basis of lattice diffusion is a simplification of the rather complex nature of these alloys. All of the alloys in Table 1 are strengthened by the formation of one or more second phases, the amount of which depends upon heat treatment.[3-10] Two of these alloys (Nimonic 105 and Udimet 720Li) have very significant amounts of a second phase (gamma prime). Thus, a more comprehensive phase-based treatment of diffusion coefficients may be warranted. However, for the calculations that follow (for Haynes 230 and Inconel

740), the values used for the lattice diffusion coefficients are ones from the FCC phase at the Cr content of the alloy (Fig. 1).

Grain boundary diffusion coefficients are estimated based on the work of Paul *et al.*[21] where lattice and grain boundary diffusion coefficients were determined for Inconel 800 (where a grain boundary width of 0.5 nm was used). The estimate uses the same ratio of grain boundary diffusion to lattice diffusion that was found for Inconel 800, and uses the same grain boundary width of 0.5 nm. This ratio is given by Eq. 14:

$$\frac{D_{Cr}^{gb}}{D_{Cr}^{L}} \cong \exp\left(\frac{12412}{T} - 1.7203\right) \qquad (14)$$

HYPOTHETICAL SUPERHEATER-STEAM PIPE-HP TURBINE STEAM PATH

The combination of gas evaporation of $CrO_2(OH)_2$, gas saturation of $CrO_2(OH)_2$, and Cr depletion in the alloy is illustrated in Fig. 2. Figure 2 represents one section of superheater (SH) tubing or steam pipe of cell length L. The bulk partial pressure of $CrO_2(OH)_2$ coming into the cell is $P_{CrO2(OH)2}°$. Evaporation within the cell at rate k_e raises the outgoing $P_{CrO2(OH)2}°$ by the amount released by evaporation and is shown in Eq. 15.

$$P^{\circ}_{CrO_2(OH)_2} = P^{\circ}_{CrO_2(OH)_2} + \frac{4k_e LRT}{duM_{CrO_2(OH)_2}} \qquad (15)$$

The effects of saturating the gas phase with $CrO_2(OH)_2$ can then be calculated along the length of a SH tube or steam pipe by combining many cells together. A hypothetical arrangement of a 100 m long, 0.05 m I.D., SH that leads into a 50m long, 0.3 m I.D., steam pipe that leads to a high pressure (HP) turbine is illustrated in Fig. 3. The temperature profile and steam velocities are shown on the left-hand axis, while the evaporation rate is shown on the right-hand axis. The SH and steam pipe each consisted of 160 cells of the type shown in Fig. 2. Saturation results in an 80% reduction in the evaporation rate at the HP turbine.

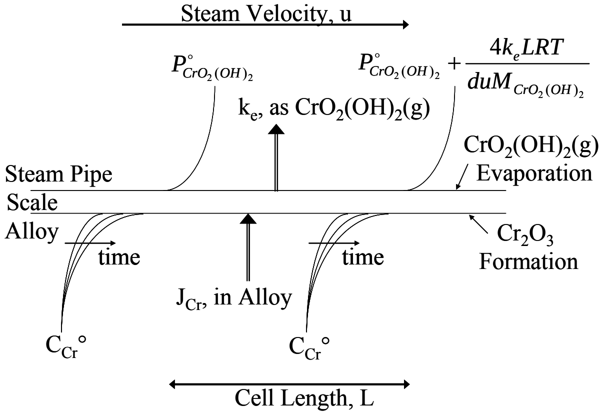

Figure 2. The combination of gas evaporation of $CrO_2(OH)_2$, gas saturation of $CrO_2(OH)_2$, and Cr depletion in the alloy is illustrated. This represents one section of superheater tubing or steam pipe of cell length L.

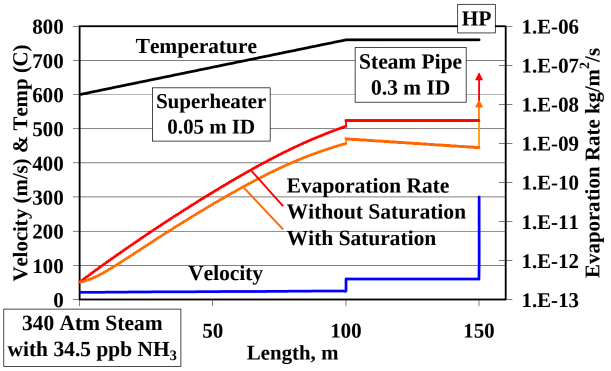

Figure 3. The effects of gas saturation is shown for a hypothetical arrangement of a 100m long SH that leads into a 50m steam pipe that leads to a high pressure (HP) turbine. Saturation results in an 80% reduction in the evaporation rate at the HP turbine.

The time for the alloy Cr level to reach zero at the scale-metal interface, using Eq. 12, is shown in Fig. 4 for the same conditions as in Fig. 3 (and using saturated values for k_e). Haynes 230 was the alloy used. At these conditions, the chromia evaporation at the HP turbine blade is expected to be so great as to deplete the alloy surface of Cr in a few days. The steam pipe inlet is the area of next concern with the time to zero Cr at the alloy surface being predicted to be about 1 year.

The very high temperatures and total pressures of Figs. 3-4 match that of the U. S. Department of Energy's goals of 760 °C and 340 atm. The impact of evaporation at lower temperatures can be seen in Fig. 5, where similar procedures are used to estimate the time it takes for the surface concentration of Cr in the alloy to reach zero. In all cases the SH inlet temperature was taken to be 600 °C. Below 600 °C, ferritic alloys, which would not be expected to form chromia scales, would typically be used.

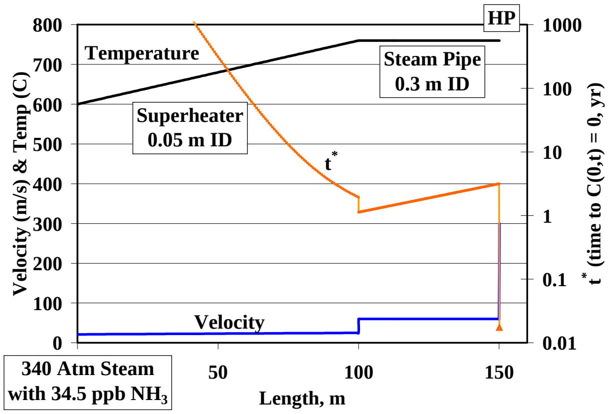

Figure 4. The predicted time for the Cr level at the scale-metal interface to reach zero.

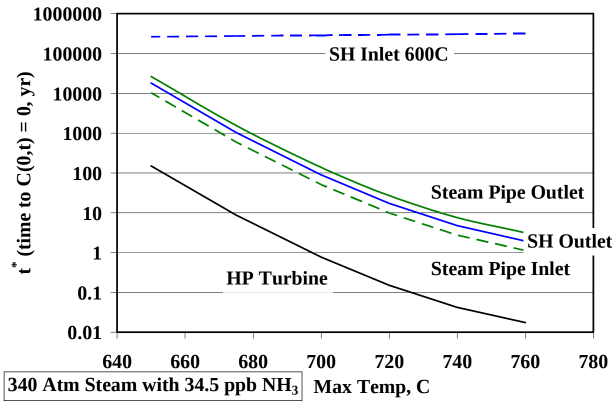

Figure 5. The effects of temperature on the estimate of the time it takes for the surface concentration of Cr in the alloy to reach zero, at 340 atm.

Figure 5 shows why chromia evaporation is not considered to be of much concern in existing steam boilers and turbines. Modern advanced steam cycles are currently no higher than 630 °C, so the time to breakaway oxidation (for which the time for C(0,t) to reach 0 is being used as an estimate) is well beyond the life span of the boiler or turbine. Another factor limiting chromia evaporation in modern advance steam cycles is that ferritic steels are extensively used, and they do not form pure chromia scales. So the activity of Cr is lower in the scales, which from Eq. 1 lowers the partial pressure of $CrO_2(OH)_2(g)$, which in turn decreases chromia evaporation (Eq. 8).

UPDATED THERMODYNAMICS

Subsequent to the development of the reactive evaporation model given above has been the examination of the thermodynamic study of $CrO_2(OH)_2(g)$ done by Opila *et al.*,[22] where it was concluded that difficulties in accurately measuring all of the released $CrO_2(OH)_2$ may have resulted in earlier studies underreporting the amount of chromia evaporation. Compared to the thermodynamic data of Gindorf,[13] the usage of the Opila *et al.* data[22] leads to the prediction of higher evaporation rates. A reexamination of the reactive evaporation model has led to two refinements that bring the predicted evaporation rates, using the Opila thermodynamic data, close to the observed rates. The first refinement is the use of a larger diffusion volume term for $CrO_2(OH)_2(g)$ in the expression for the diffusion coefficient of $CrO_2(OH)_2(g)$ in the gas stream.[2] A model of the $CrO_2(OH)_2(g)$ molecule in the Opila work[22] has a bond length of Cr-H that leads to an estimate of the diffusion volume of 32.9 cm^3/mol instead of 10.3 cm^3/mol that was used based on the Cr-O bond in CrO.[2] The second refinement was to reexamine the assumption that the activity of chromia in the oxide scale was equal to 1 (a pure chromia scale). As chromia is removed from the oxide scale, any impurities will remain and be concentrated at the outer surface of the scale. An activity of chromia equal to 0.05, combined with a value of 32.9 cm^3/mol for the diffusion volume, brings the model's prediction of evaporation rates close to the observed rates for Haynes 230 and Inconel 625. The value of 0.05 for the chromia activity compares with a chromia activity of 0.0006 for $MnCr_2O_4$ (ref 23) that can form when the Mn content is high enough to form a continuous outer layer of the spinel scale. Variations in chromia activity also allows for an explanation for cases where less evaporation is observed. An example of this is Inconel 740 (ref 24), where the evaporation rates were either very low (consistent with a chromia activity on the order of 0.0006, or were initially similar to that found on Hayes 230 or Inconel 625 (ref 2) and then later switched to the lower rate. High concentrations of Ti and Mn were found on the outer part of the oxide scale on Inconel 740, which is a further indication of lower chromia activity. Table 1 shows that Inconel 740 has much higher Ti levels than Haynes 230 or Inconel 625.

FUTURE WORK

Laboratory testing of corrosion behavior is ideally performed in the same environment as the expected service conditions. In the case of USC steam turbine environments, such laboratory tests at high temperatures, pressures, and steam velocities would be prohibitively expensive. Alternative laboratory tests were designed to show specific corrosion mechanisms of the type seen under service conditions. Two types of experiments are planned. The first will have exposures to steam at high pressures and temperatures in an autoclave. The second will be the use of an erosion test rig, used without an erodent, to expose samples in moist air with a relatively high gas velocity. The samples rotate on the perimeter of the disk, which results in an effective gas velocity of up to 40 m/s.

The autoclave tests in high-temperature and high–pressure steam should show the type of chromia scale formation that would occur without appreciable chromia evaporation. The rotating disk tests should show similar evaporation rates that would be expected in the USC HP turbine. The basis for these two predictions is in Figure 6, which shows the expected evaporation rates for the USC HP turbine (without saturation effects), low gas flow laboratory experiments (for a wide range of oxygen partial pressures), and rotating disk experiments (in air with 3%-50% H_2O). Figure 6 indicates that exposures in steam (with low oxygen contents) at low laboratory-type flows would not result in measurable evaporation rates. However, 40 m/s exposures in air with 3% to 50% H_2O should result in evaporation rates that are similar to those expected to occur in USC HP turbines. These rotating disk exposures will serve as validation of the chromia evaporation model in turbulent conditions.

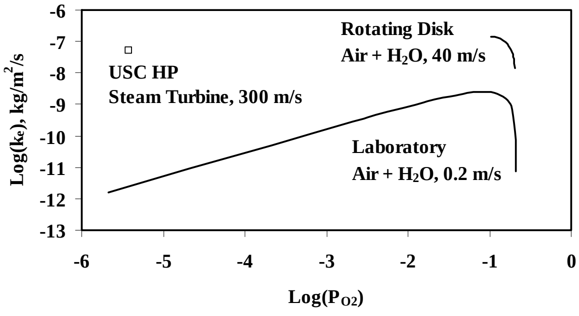

Figure 6. A comparison, at 760 °C, of evaporation rates for USC HP steam turbine conditions (without saturation effects), low gas flow laboratory experiments (for a wide range of oxygen partial pressures), and rotating disk experiments (in air with 3%-50% H_2O).

CONCLUSIONS

A methodology that was developed earlier to calculate Cr evaporation rates from Cr_2O_3 with a flat planar geometry,[2] was expanded upon to allow for interior cylindrical geometries, and to allow for the effects of $CrO_2(OH)_2$ saturation within the gas phase. This approach was combined with Cr diffusion calculations within the alloy (with a constant flux of Cr leaving the alloy from evaporation) to predict Cr concentration profiles as a function of exposure time and to predict the time until the alloy surface concentration of Cr reaches zero. This time is a rough prediction of the time until breakaway oxidation.

A hypothetical super heater (SH) tube, steam pipe, and high pressure (HP) turbine steam path was assembled and examined with the methodology. At the U. S. Department of Energy's goals of 760 °C and 340 atm, the time until breakaway oxidation was predicted to be quite short for the turbine blade, and of concern within the steam pipe and the higher temperature portions of the SH tube. The predicted time until breakaway oxidation increases dramatically with decreases in temperature and total pressure.

Incorporation of the Opila *et al.* thermodynamic data[22] into the model has allowed for differences in chromia activity at the outer portion of the oxide scale, which result from alloy composition differences, to account for differences in observed evaporation rates.

REFERENCES

1. R. Viswanathan, J.F. Henry, J. Tanzosh, G. Stanko, J. Shingledecker, B. Vitalis, and R. Purgert, "U.S Program on Materials Technology for Ultra-Supercritical Coal Power Plants," *Journal of Materials Engineering and Performance*, 14 (2005), 281-292.
2. Haynes 230 Alloy, H-3135C (Kokomo, IN: Haynes International, 2008).
3. Haynes 282 Alloy, H-3172A (Kokomo, IN: Haynes International, 2008).
4. Inconel Alloy 617, SMC-029 (Huntington, WV: Special Metals Corporation, 2005).
5. Inconel Alloy 625, SMC-063 (Huntington, WV: Special Metals Corporation, 2006).
6. Inconel Alloy 718, SMC-045 (Huntington, WV: Special Metals Corporation, 2007).
7. Inconel Alloy 740, SMC-090 (Huntington, WV: Special Metals Corporation, 2004).
8. Nimonic Alloy 90, SMC-081 (Huntington, WV: Special Metals Corporation, 2007).
9. Udimet Alloy 720, SMC-106 (Huntington, WV: Special Metals Corporation, 2004).
10. G.R. Holcomb, "Calculation of Reactive Evaporation Rates of Chromia," *Oxidation of Metals*, 69 (2008), 163-180.
11. H. Asteman, J.-E. Svensson, L.-G. Johansson, and M. Norell, "Indication of Chromium Oxide Hydroxide Evaporation During Oxidation of 304L at 873 K in the Presence of 10% Water Vapor," *Oxidation of Metals*, 52 (1999), 95-111.
12. H. Asteman, J.-E. Svensson, M. Norell, and L.-G. Johansson, "Influence of Water Vapor and Flow Rate on the High-Temperature Oxidation of 304L; Effect of Chromium Oxide Hydroxide Evaporation," *Oxidation of Metals*, 54 (2000), 11-26.
13. C. Gindorf, K. Hilpert, and L. Singheiser, "Determination of Chromium Vaporization Rates of Different Interconnect Alloys by Transpiration Experiments," *Solid Oxide Fuel Cells (SOFC VII)*, Proceedings Vol. 2001-16, ed. H. Yokokawa and S.C. Singhal (Pennington, NJ: Electrochemical Society, 2001), 793-802.
14. R.H.S. Winterton, "Where did the Dittus and Boelter Equation Come From?" *International Journal of Heat and Mass Transfer*, 41 (1998), 809-810.
15. Frank P. Incropera and David P. DeWitt, *Fundamentals of Heat and Mass Transfer*, 5th Ed. (New York, NY: John Wiley & Sons, 2001), 268-270, 491-492, 508.
16. B.S. Petukhov, "Heat Transfer and Friction in Turbulent Pipe Flow with Variable Physical Properties," *Advances in Heat Transfer*, Vol 6, ed. T.F. Irvine and J.P. Hartnett (New York, NY: Academic Press, 1970), 503–564.
17. X. Peng, J. Yan, Y. Zhou and F. Wang, "Effect of Grain Refinement on the Resistance of 304 Stainless Steel to Breakaway Oxidation in Wet Air," *Acta Materialia*, 53 (2005), 5079-5088.
18. Dictra, Diffusion Simulation Software, Version 24 (Stockholm, Sweden: Thermo-Calc Software AB, 2006).
19. N. Saunders, *Ni-DATA*, Version 7 (Surrey, UK: Thermotech Ltd, Surrey Technology Centre, 2000).
20. *MOB2*, Mobility Database, Version 2.0 (Stockholm, Sweden: Royal Institute of Technology, Foundation of Computational Thermodynamics, 1999).
21. A.R. Paul, K.N.G. Kaimal, M.C. Naik and S.R. Dharwadkar, "Lattice and Grain Boundary Diffusion of Chromium in Superalloy Incoloy-800," *Journal of Nuclear Materials*, 217 (1994), 75-81.
22. E. J. Opila, D. L. Myers, N. S. Jacobson, I. M. B. Nielsen, D. F. Johnson, J. K. Olminsky, and M. D. Allendorf, "Theoretical and Experimental Investigation of the Thermochemistry of $CrO_2(OH)_2(g)$," *J. Phys. Chem. A*, 111 (2007), 1971-1980.
23. G. R. Holcomb, D. E. Alman, "The Effect of Manganese Additions on the Reactive Evaporation of Chromium in Ni-Cr Alloys," *Scripta Materialia*, 54 (2006), 1821-1825.
24. G. R. Holcomb, D. E. Alman, Ő. N. Doğan, J. C. Rawers, K. K. Schrems, and M. Ziomek-Moroz, "Steam Turbine Materials and Corrosion," *Proceedings of the 21st Annual Conference on Fossil Energy Materials*, Knoxville, TN, April 30-May 1, 2007 (U.S. Department of Energy, Office of Fossil Energy, Advanced Research Materials) 2007.